Report Documentation Page

Form Approved
OMB No. 0704-0188

1. REPORT DATE	2. REPORT TYPE	3. DATES COVERED
2011		**00-00-2011 to 00-00-2011**

4. TITLE AND SUBTITLE	5a. CONTRACT NUMBER
A Numerical Study of Novel Drag Reduction Techniques for Blunt Bodies in Hypersonic Flows	5b. GRANT NUMBER
	5c. PROGRAM ELEMENT NUMBER
6. AUTHOR(S)	5d. PROJECT NUMBER
	5e. TASK NUMBER
	5f. WORK UNIT NUMBER
7. PERFORMING ORGANIZATION NAME(S) AND ADDRESS(ES) **Missouri University of Science and Technology,1870 Miner Circle,Rolla,MO,65409**	8. PERFORMING ORGANIZATION REPORT NUMBER
9. SPONSORING/MONITORING AGENCY NAME(S) AND ADDRESS(ES)	10. SPONSOR/MONITOR'S ACRONYM(S)
	11. SPONSOR/MONITOR'S REPORT NUMBER(S)

12. DISTRIBUTION/AVAILABILITY STATEMENT
Approved for public release; distribution unlimited

13. SUPPLEMENTARY NOTES

14. ABSTRACT

Numerical simulations of a full three-dimensional hemispherical body in hypersonic flow are conducted and innovative techniques involving forward injection of gas from the stagnation point of the sphere are investigated; techniques include annular (ring) and swirled injection both with and without upstream energy deposition. Objectives of the analysis are the assessment of 1) drag reductions achieved on the blunt body (including the detrimental drag effect caused by the forward-facing injection itself) and 2) stability characteristics of the jet. Studies are conducted at free-stream Mach numbers of 10 and 6.5 at standard atmospheric conditions corresponding to 30 km altitude. While centered forward injection without upstream energy deposition is confirmed to be highly unstable either with or without swirl, annular ring injection exhibits a stabilizing influence on the jet. Energy deposition upstream of the body is shown to significantly enhance stability and penetration of the forward injection jet for all techniques.

15. SUBJECT TERMS

16. SECURITY CLASSIFICATION OF:			17. LIMITATION OF ABSTRACT	18. NUMBER OF PAGES	19a. NAME OF RESPONSIBLE PERSON
a. REPORT	b. ABSTRACT	c. THIS PAGE			
unclassified	**unclassified**	**unclassified**	**Same as Report (SAR)**	**45**	

A NUMERICAL STUDY OF NOVEL DRAG REDUCTION TECHNIQUES FOR BLUNT BODIES IN HYPERSONIC FLOWS

by

CHRISTOPHER DAVID MARLEY

A THESIS

Presented to the Faculty of the Graduate School of the

MISSOURI UNIVERSITY OF SCIENCE AND TECHNOLOGY

In Partial Fulfillment of the Requirements for the Degree

MASTER OF SCIENCE IN AEROSPACE ENGINEERING

2011

Approved by

David W. Riggins, Advisor
Serhat Hosder
Kakkattukuzhy M. Isaac

ABSTRACT

Numerical simulations of a full three-dimensional hemispherical body in hypersonic flow are conducted and innovative techniques involving forward injection of gas from the stagnation point of the sphere are investigated; techniques include annular (ring) and swirled injection both with and without upstream energy deposition. Objectives of the analysis are the assessment of 1) drag reductions achieved on the blunt body (including the detrimental drag effect caused by the forward-facing injection itself) and 2) stability characteristics of the jet. Studies are conducted at free-stream Mach numbers of 10 and 6.5 at standard atmospheric conditions corresponding to 30 km altitude. While centered forward injection without upstream energy deposition is confirmed to be highly unstable either with or without swirl, annular ring injection exhibits a stabilizing influence on the jet. Energy deposition upstream of the body is shown to significantly enhance stability and penetration of the forward injection jet for all techniques.

ACKNOWLEDGMENTS

At this time, I would like to thank my advisor, Dr. David Riggins. This work was possible only with his support. It was Dr. Riggins' initial ideas regarding drag reduction that sparked this research. His insights into the physics of high speed flows, along with his knowledge of computational fluid dynamics, helped me greatly to progress in this work. He invested much of his time in helping me and I am very grateful for that.

As well, I would like to thank my committee members, Dr. Serhat Hosder and Dr. Kakkattukuzhy Isaac. Dr. Hosder's knowledge of computational fluid dynamics as well as his general knowledge of high speed aerospace systems was very helpful. Also, I want to say thanks to all my friends and family. Specifically, thanks to Mom and Dad, and to Joe and to Parimal.

Lastly, this work was partially supported by the Air Force Office of Scientific Research through the AFRL Summer Researchers Program. Specifically, I would like to thank Dr. David Moorhouse and Dr. Jose Camberos of the Air Vehicles Directorate at Wright Patterson Air Force Base for their support.

TABLE OF CONTENTS

LIST OF ILLUSTRATIONS

NOMENCLATURE

Symbol	Description
A_j	Crosssectional Area of Jet
D_{mod}	Pressure Drag on Body after Modification
D_{ref}	Pressure Drag on Body without Modification
d	Diameter of hemisphere
d_j	Effective Jet Diameter Based on Crosssectional Area
I	Number of Iterations
l	Location of Energy Deposition Forward of Body
M_j	Mach Number of Jet
M_∞	Free-Stream Mach Number
$\dot{m}_j$	Mass Flow Rate of Jet
p	Static Pressure
p_s	Stagnation Pressure
p_j	Static Pressure of Jet
p_{tj}	Total Pressure of Jet
$\dot{Q}$	Rate of Free-Stream Energy Deposition
S	Power Effectiveness Ratio
s	Surface Coordinate
T_j	Jet Thrust
T_{tj}	Total Temperature of Jet
T_∞	Free-Stream Static Temperature
u_j	Jet Velocity in Axial Direction
V_∞	Free-Stream Velocity
Δ	Shock Standoff Distance

1. INTRODUCTION

Achieving practical hypersonic flight has been a focus of research in industry, academia and government laboratories across the world for more than sixty years. Some hypersonic applications involving missile nose cones and conventional reentry vehicles are generally considered mature in terms of the existence of established practices and techniques relevant to operational vehicles. However, despite this relatively long history associated with hypersonics, there remain significant challenges (and related opportunities) in terms of both the performance and the operability of existing and proposed hypersonic systems [1]. A fundamental design challenge of interest for hypersonic cruisers and accelerators (particularly air-breathing vehicles) is the inherently low thrust minus drag performance margins across the operating envelopes of such vehicles. The focus of the present work is on the development and assessment of innovative approaches for the reduction of the drag experienced by hypersonic vehicles. Techniques involving forward-facing injection from relatively blunt hypersonic leading edges, both with and without upstream energy deposition, are numerically examined for an axi-symmetric blunt-nosed body in hypersonic flow. The specific objective of the paper is to provide an assessment of the use of forward-facing annular ring injection for drag reduction and jet stabilization from the blunt fore-bodies of axi-symmetric leading edges; also of interest is the effectiveness of swirling the forward-facing injected gas. These concepts will be examined with and without upstream energy deposition. Such techniques are conjectured to potentially minimize the mass flow rate required to achieve significant drag reductions (as compared to a conventional single stream injector). Of equal interest for these cases are the stability characteristics of the innovative forward facing ring injector concepts in terms of maintaining upstream penetration of the injected stream. This then requires full three-dimensional simulations of the flow-fields (i.e. no assumptions of symmetry are made in the present work).

The high drag associated with hypersonic flight has dictated that hypersonic cruisers and accelerators have high fineness ratios and sharp leading edges which minimize wave drag. Figure 1.1 shows a comparison between a conventional hypersonic vehicle configuration and a new hypothetical configuration. Figure 1.1a shows a sketch

of a typical wave-rider/lifting body type of hypersonic air-breathing vehicle (such as the X-43). The design is characterized by a highly integrated airframe and propulsion system and sharp leading edges. The oblique shocks originating from the sharp vehicle nose and fore-body sufficiently compress the air entering the engine for supersonic or dual-mode combustion, but with large reduction of inlet/fore-body drag and total pressure loss as compared to that which would be experienced by a blunt-nosed fore-body. This reliance on oblique shocks mandates a high structural/aerodynamic fineness ratio for the vehicle (sharp small-radius nose curvature and long inlet/fore-body lengths).

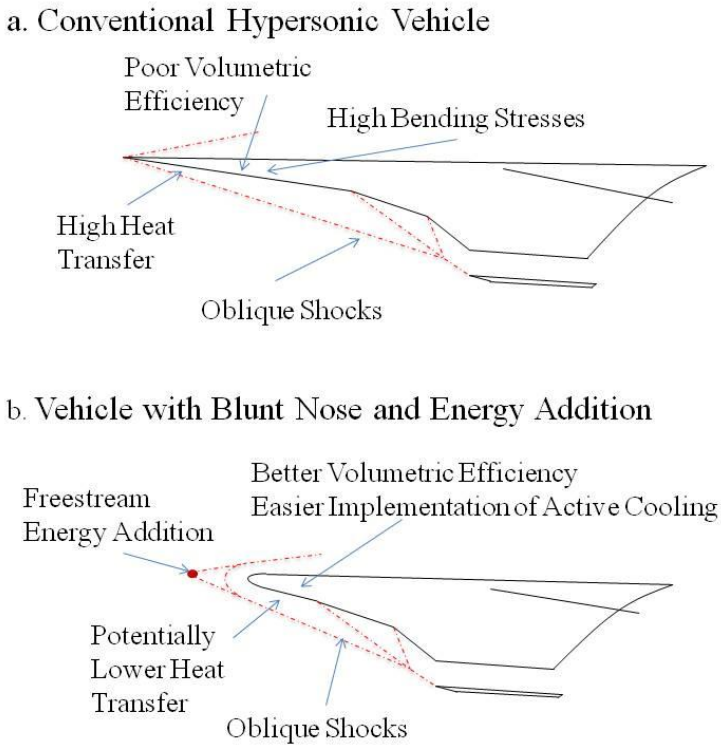

Figure 1.1. Comparison of Hypersonic Vehicle Configurations. a) Conventional Configuration. b) Modified Blunt Nose Configuration with Energy Deposition.

While drag reduction and pressurization for lift on the fore-body/inlet surface are therefore achieved, there are a number of significant detrimental effects as well. Specifically, high heat transfer rates to the vehicle result due to the proximity of the shocks to the vehicle surface; temperature is high and thermal gradients large in such

layers. In addition, for thin sharp (high structural fineness ratio) noses or leading edges, the small volume associated with the nose makes the design of active cooling techniques for the vehicle nose or leading edge a challenge and also limits the materials that can be used in constructing the vehicle. Another disadvantage of the high fineness ratio non-symmetric lifting-body/wave rider concept is the large positive (nose up) pitching moments generated at vehicle orientations for maximum thrust production as well as resultant bending stresses encountered on the vehicle. This latter effect introduces the need for structural reinforcement in order to lessen flexure and to provide integrity to the airframe. In addition, to counter pitching moments associated with the high aerodynamic fineness ratio of the vehicle, the vehicle must have sufficient control surfaces and mass balancing which can result in sub-optimal designs with reduced performance and operability capabilities.

The sharp leading edges and high aerodynamic fineness ratio characterizing hypersonic cruisers and accelerators are in contrast to that seen for reentry vehicles. For such vehicles blunt fore-bodies are useful for ablative/cooling subsystems, due to increased vehicle volumetric efficiency. Overall heating to the nose surfaces can, in fact, actually be less than that experienced by a long sharp-nosed fore-body due to fluid dynamics associated with the subsonic zone downstream of the normal shock. Blunt noses and leading edges, often utilized in spacecraft launch and reentry vehicles and high speed missiles, are thus less susceptible than sharp noses and leading edges to some of the adverse effects associated with cooling requirements and system-level effects, as described above for hypersonic cruisers and accelerators. Unfortunately, the strong bow shocks formed by a blunt body cause very high surface pressures on the forward facing surfaces, hence very large drags. For reentry vehicles, high drag is actually desirable in order to decelerate the vehicle within structural, control and heating limits. Also, even for accelerative atmospheric flight systems, the large thrust to drag margins associated with rocket propulsion systems can generally overcome the high drag experienced by the blunter noses and leading edges on missiles and launch vehicles. Nevertheless, for all applications, if the high drag associated with hypersonic flow over blunt noses and leading edges can be reduced and/or controlled utilizing innovative techniques, the vehicle design will require less fuel and be more intrinsically efficient. For hypersonic

air-breathing vehicles which have inherently low thrust minus drag margins, advantages would be realized if designs could have blunter noses and leading edges than those currently required and yet still maintain the lower drags associated with sharp high-fineness ratio systems. In addition, it would be advantageous to increase volumetric efficiency (minimize adverse heating and structural effects from the standpoint of the overall system).

Experiments and numerous numerical studies have shown that volumetric heating of regions of the flowfield achieved by depositing energy through microwaves, lasers, electron beams, electric arcs, plasmas or other means can result in significant reductions in shock wave drag via the mechanism of flow-field modification of those shocks [2]. Numerical studies indicate that energy deposition in the free-stream of a two dimensional blunt body at hypersonic speeds can reduce drag by up to 70 percent [3]. A sketch of a hypersonic vehicle which incorporates the effects and advantages of upstream deposition of energy is shown in Figure 1.1b. As an example of a previous numerical study which focused on vehicle level performance achieved utilizing such techniques see Taylor [4]. Studies (both experimental and numerical) have also shown that forward facing mass injection has the ability to significantly reduce drag on blunt bodies by increasing the shock standoff distance and replacing the normal shock with weaker oblique shocks [5]. Studies have also been done which combined both upstream injection and energy deposition with significant improvements in drag reduction, heat transfer and jet stability characteristics. This paper extends earlier work on forward-facing injection and energy deposition upstream of blunt bodies by analyzing the use and performance of an axi-symmetric annular ring injector as well as imposing swirl (rotation) in the injectant. The current studies utilize a three-dimensional approach without the use of any assumed symmetry boundaries; hence can be used to study jet instability and stabilization.

The organization of this thesis is as follows: Section 2 provides a survey of wave drag reduction techniques on blunt bodies in hypersonic flows, including structural spikes, forward facing injection of mass, upstream deposition of energy and combination of the techniques. Section 3 discusses the computational methodology used in the present study and details the comparison of base-line results with experimental data for forward-facing injection from a blunt body. Section 4 is the discussion of results obtained in

which a variety of techniques involving both forward-facing injection and energy deposition for an axi-symmetric blunt-nosed body are numerically analyzed. These techniques include both swirling injection and annular-ring injection. Section 5 provides a summary of results.

2. SURVEY OF BLUNT BODY WAVE DRAG REDUCTION TECHNIQUES

This section provides a survey of techniques and previous investigations focused on the reduction of wave drag (and heat transfer) on blunt bodies in hypersonic flows. Early studies of blunt body wave drag reduction began in the early 1940's. The realization that a blunt body, as compared to a sharp, slender body, can actually result in relatively less heat transfer to a vehicle during reentry resulted in a paradigm shift in spacecraft design [1]. The prospect of utilizing blunt bodies in hypersonic flows caused engineers to investigate methods of reducing the drag experienced by such bodies. In this section, the advantages and disadvantages of several techniques for drag reduction on blunt bodies, including structural spikes, forward mass injection and free-stream energy deposition, will be reviewed in terms of previous work.

2.1. STRUCTURAL SPIKE

One method used for wave drag reduction on blunt bodies is the structural spike as shown in Figure 2.1. The spike works by creating a region of separated flow adjacent to the spike, just forward of the nose. In fact, in early NACA publications, the spike was actually referred to as a "flow separation spike" [6, 7]. This region of flow separation is caused by an adverse pressure gradient in the boundary layer region of the spike. This recirculation or "dead-air" region modifies the bow shock such that the shock moves upstream. In addition there is a low dynamic pressure associated with the recirculation region which reduces the pressure on the nose of the body and hence reduces the overall drag (as well as the overall heat transfer to the body). Depending on details of the flow conditions, blunt body shape, and spike geometry, the drag on a body at hypersonic speeds can be reduced from 20 to 60 percent with a structural spike [8]. Also shown in Figure 2.1 is a comparison of different spike geometries, one of which is the aerodome. The aerodome has a large amount of flow separation induced compared to a sharp or blunt spike. A spike with an aerodome tip was successfully implemented on the nose cone of the HyCAUSE scramjet demonstration vehicle in 2007 [8].

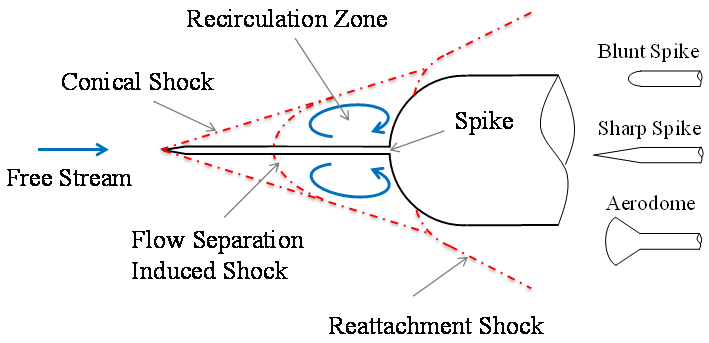

Figure 2.1. Schematic of Flowfield Induced by Structural Spike and Comparison of Spike Geometries.

Structural spikes have seen success primarily on launch vehicles and missiles. The spike has sufficiently low drag during launch and allows for high volumetric efficiency by allowing the use of a blunt body instead of a slender body. However at higher velocities the spike itself suffers from excess heat and ablation due to high stagnation temperatures, as well as high structural loading. The nose cone is a disposable element on a launch vehicle or a missile; on a cruise vehicle however, the spike would be a permanent element and the damage to the spike due to heating would be intolerable. For this reason, innovative alternatives to the structural spike have been investigated with specific interest for use in the design of airbreathing hypersonic vehicles.

2.2. MASS INJECTION

Drag reduction on blunt bodies in hypersonic flows can be achieved by the forward injection of fluid from the blunt body; generally the injection is centered at or near the stagnation point on the body surface. In theory, the structural spike is replaced by a non-structural spike, consisting of the forward penetrating jet. The mass injection technique, if successfully implemented, would avoid issues of heating and ablation experienced by a physical spike while still reducing the overall drag and heat transfer to the body. Note that when considering the overall drag reduction on a body employing a forward facing jet, the jet itself contributes to the drag. Researchers began investigating forward injection of various gases on blunt bodies at supersonic speeds in the early 1940's [5]. Gases used in these experiments included air, nitrogen, helium and even

combustible gases such as hydrogen. Figure 2.2 describes a typical mass injection system along with its typical modes of operation. Shown in Figure 2.2a is a sketch of an injection system on a blunt body.

While drag reduction was one motivation for the study of mass injection, another motivation for such experiments was to investigate the ability of mass injection of cooler and/or inert gases to reduce heat transfer to blunt bodies [9, 10]. Depending on the free-stream conditions (free-stream Mach number, total pressure, etc.) and jet conditions (gas injected, jet Mach number at exit of nozzle, jet total pressure and ratio of jet diameter to body diameter) it was found that heat transfer could be reduced by up to 40 percent [9]. Experiments also showed that when the drag generated from the forward facing jet is considered, the total drag acting on a blunt body at low supersonic speeds could be reduced by up to 20 percent [5]. One numerical study of a two-dimensional blunt body, which used a symmetry boundary condition, at a free-stream Mach number of 6.4 found the maximum drag reduction to be 40 percent [11].

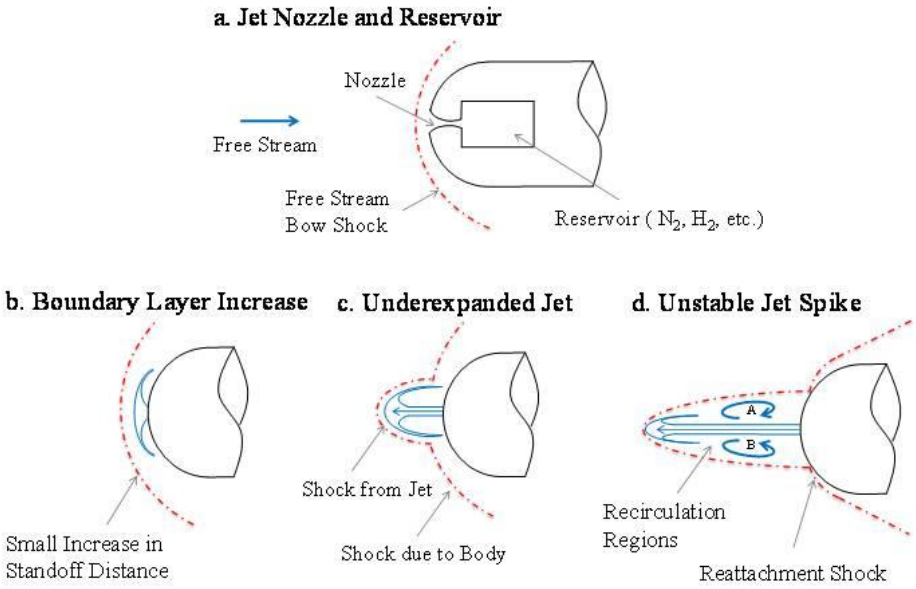

Figure 2.2. Mass Injection System and Operation. a) Sketch of Injector Nozzle and Reservoir. b-d) Distinct Modes of Injection.

Experimental investigations of forward facing injection at hypersonic speeds have identified two modes of injection [12, 13]. In one mode, shown in Figure 2.2b, the ratio of jet total pressure to the total pressure of the free-stream is low and the jet does not penetrate through the bow shock formed in front of the blunt body. Instead the injection causes the bow shock to move forward while maintaining a similar shape as the non-injection case. Note that while a jet in this first mode does not significantly alter the pressure drag, it still can have a favorable effect by increasing the size of the boundary layer and hence reducing heat transfer to the surface. As the ratio of total pressure of the jet to total pressure of the free-stream air increases, a second mode, shown in Figures 2.2c and 2.2d, is established. In this mode, the jet penetrates the initial bow shock and decelerates, turns and mixes with the free-stream. In addition to the body induced bow shock, a shock is formed by the jet where it decelerates and turns such that the total pressure of the jet matches the total pressure of the free-stream. This second mode resembles a structural spike and drag reduction similar to that obtained by a physical spike. Recirculation regions form adjacent to the jet aft of the jet induced shock (regions A and B in Figure 2.2d). These recirculation regions adjacent to the nose of the blunt body have a lower static pressure compared to the case with no jet and hence the drag force on the body is reduced. Depending on the flow conditions as well as the conditions of the jet, the shocks due to the jet can impinge on the surface of the body creating an adverse region of high pressure and heat transfer on the body.

It is important to note that the second type of forward mass injection is unstable. Experiments have revealed two modes of instability [12, 13]. In the first type, seen in Figure 2.2c, the jet penetrates through the bow shock and remains at approximately the same axial location. However, the jet oscillates randomly in the lateral directions. As the ratio of total pressure of the jet to the total pressure of the free-stream increases further, the mode of instability changes to the second type shown in Figure 2.2d. The jet penetrates even farther forward but does not remain at this new axial location. Instead it collapses back to the first type of instability and then penetrates forward again in a cyclic manner. In both cases, the instability is due to pressure variations in the recirculation regions on either side of the jet. The reason for the cyclic motion in the second type of instability is the larger area over which the pressure acts on the jet. This larger pressure

difference moves the jet farther from the centerline and resultant pressure from the free-stream then pushes the jet back towards the body.

2.3. ENERGY DEPOSITION

Another method used for achieving drag reduction for blunt bodies at hypersonic flight Mach numbers is energy deposition. A small volume of air forward of the vehicle can conceptually be heated by various means including microwaves, microwave generated plasma, magnetohydrodynamic effects, electron beams or localized plasma-assisted surface combustion [14]. This heating couples with the body and transforms the existing shock wave formation forward of the blunt body into a system similar to that seen with a structural spike and mass injection. A sketch of the flow-field resulting from energy deposition is shown in Figure 2.3. The volumetric heating causes a temperature rise and hence the Mach number in this small volume forward of the body drops; the flow can become subsonic. Due to this disturbance in the otherwise supersonic flow-field, the flow is deflected and either a conical or parabolic shock forms depending on the location of the deposition with respect to the body as well as the rate of heat addition [14]. The Mach number in the region behind the conical shock is reduced with respect to the free-stream Mach number and hence the Mach number 'observed' by the body is reduced. The end result is an increase in the shock standoff distance which leads to a reduction in pressure on the surface of the blunt body and hence a reduction in drag experienced by the blunt body [15].

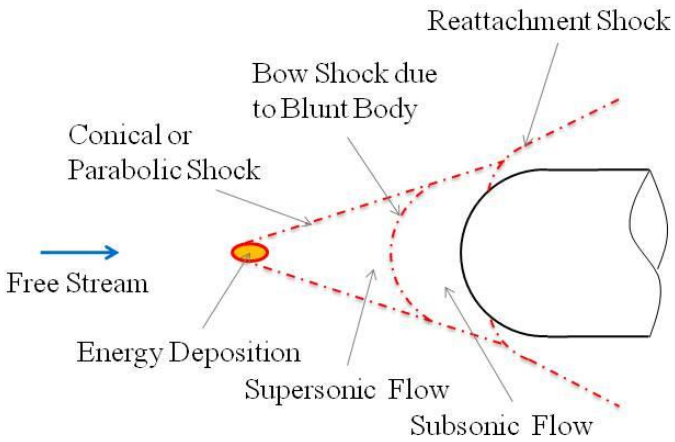

Figure 2.3. Sketch of Flow-Field Induced by Energy Deposition Forward of Blunt Body.

Note that if the shocks originating from the energy deposition impinge on the body, any reduction in pressure at the nose of the body could be canceled out and an increase in the overall drag could occur. An important distinction in the flow-field resulting from energy deposition as compared to a structural spike or mass injection is often the lack of a recirculation zone caused by the presence of the spike or jet. The lack of a deformable shear surface such as a jet causes the flow-field resulting from energy deposition to be much more stable. Parameters of energy deposition include the rate of energy addition as well as its location and shape. One numerical study of energy deposition near the surface of a hypersonic vehicle revealed that the shape of the energy addition region had little effect on the resulting flow-field [16]. A numerical study using an axi-symmetric boundary condition to investigate drag reduction on a blunt body at Mach 10 shows a maximum drag reduction of 70 percent with an energy deposition rate of 800 W compared to the baseline case with no energy addition [3]. This same study demonstrated a strong dependency of the observed drag reduction as a function of the location of energy deposition forward of the body. The drag decreases as the deposition distance forward of the nose increases until at some specific location the drag reaches a minimum. As the deposition location is moved further forward, the shock wave formed in the vicinity of the energy deposition separates from the shock system associated with the blunt body itself and the standoff distance of the bow shock begins to decrease with attendant increase in drag force experienced by the blunt body. Flow-field modification using focused energy deposition, as well as a combination of energy deposition and mass injection, has a very promising future and for further details, the reader is referred to Riggins et al. [17].

3. COMPUTATIONAL METHODOLOGY AND COMPARISON WITH EXPERIMENTAL DATA

The primary purpose of the current investigation is to study the drag reduction and stability characteristics of forward mass injection on three-dimensional blunt bodies and to assess possible techniques for enhancing the drag reduction and the stability of the forward penetrating jet. Specifically, one objective of the study is to assess the use of a swirl velocity component imposed on the injectant at the injection orifice plane. This then demands a full three-dimensional solution as opposed to a (2-D) axi-symmetric solution. The instability associated with mass injection is due to pressure variation on the jet from side to side as discussed earlier. An axi-symmetric boundary condition along the stagnation streamline generally forces the solution to be stable (i.e. prevents side to side motion or movement of the jet). In this study, the code used is the VULCAN (Viscous Upwind aLgorithm for Complex flow ANalysis) computational fluid dynamics solver developed at NASA Langley for studying high speed flows. A sketch of the computational model is shown in Figure 3.1.

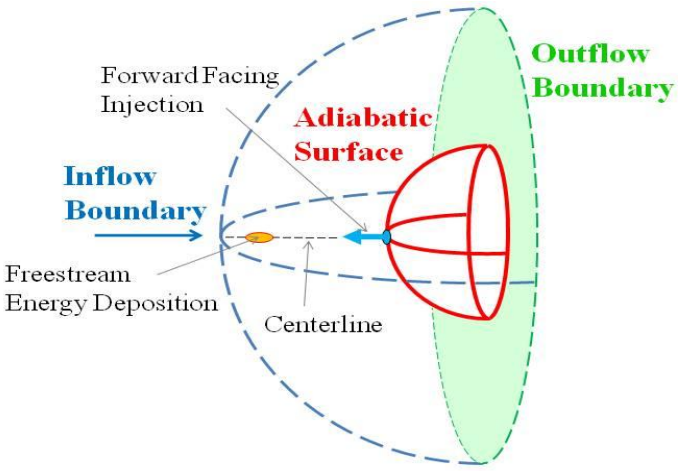

Figure 3.1. Computational Model Developed for Study of Drag Reduction Techniques on Hemispherical Body.

3.1. DISCRETIZATION

VULCAN supports parallel processing and requires structured, PLOT3D grids. The surface mesh of the hemispherical nose studied in this paper is shown in Figure 3.2. The mesh is referred to as a spherical cube; the *x'*-, *y'*- and *z'*-coordinates on the surface of a unit cube are generated and then appropriate equations are used to map these coordinates to the *x*-*y*- and *z*-coordinates on the surface of a unit sphere. The coordinates are then scaled such that the diameter of the hemisphere is 0.02 m. This method of grid generation is used to avoid excessive skew at the poles of the sphere experienced with other sphere meshing techniques. The maximum skew of the surface mesh, defined as the cosine of the acute angle between the edges at a corner of a quadrilateral element, is found to be only 0.83. The three-dimensional domain in which the flow-field is to be solved is then generated by protruding the surface mesh out in the direction normal to the sphere as shown in Figure 3.3. A total of ten grid blocks are generated and the flow-field in each block is then solved on a separate processor using the VULCAN parallel processing capability. Blocks 1 through 4 are generated from Faces 1 through 4. Blocks 6 through 10 are generated from Face 5 and are suitably stacked on top of one another. The *i*- and *j*-directions are taken to be the tangential directions on the sphere and the *k*-direction is taken to be normal to the sphere. For the base-line grid, Blocks 1 through 4 contain 23 x 69 x 61 nodes and Blocks 4 through 10 contain 69 x 69 x 21 nodes. The nodes are clustered on the surface at the center of the sphere (i.e. the stagnation region) to provide high grid resolution near the region of mass injection or energy deposition. The nodes are also clustered at the surface of the sphere in the k-direction in order to capture transport phenomenon although heat transfer and viscous effects are not considered in this study which focuses primarily on pressure drag reduction and injection stability.

To ensure grid independence, the solution using the base-line grid defined above is compared to solutions using a coarse grid with approximately half the nodes as the base-line grid as well as a fine grid with approximately twice the number of nodes as the base-line grid. The case studied in the grid independence test is a base-line case with no injection or free-stream energy addition at a free-stream Mach number of 6 and free-stream pressure and temperature corresponding to standard atmospheric conditions at 30 km altitude. After converging to the steady solution, the pressure drag using the base-line

grid was found to be 8.88 N. The pressure drag obtained with the coarse grid was found to be 1.2 percent lower than the drag using the base-line grid, where as the pressure drag using the fine grid was only 0.4 percent higher.

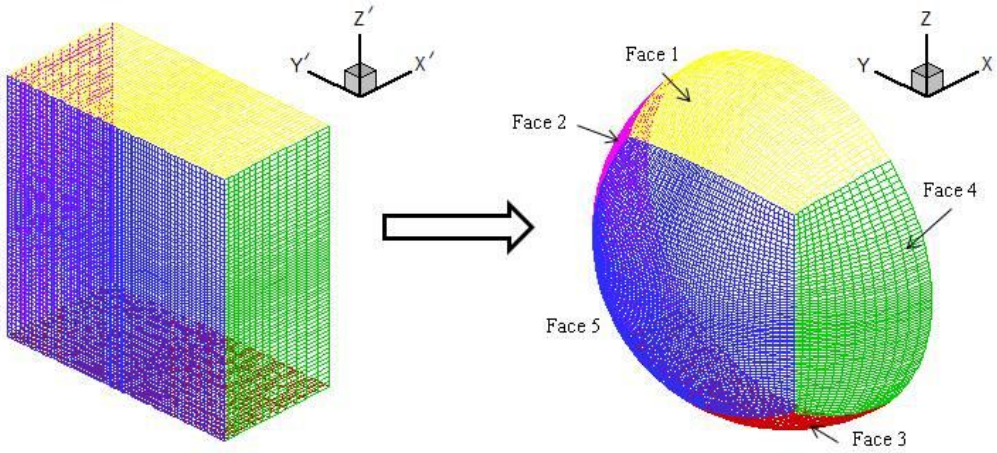

Figure 3.2. Mapping of the Surface Mesh on a Half-Cube to a Hemisphere.

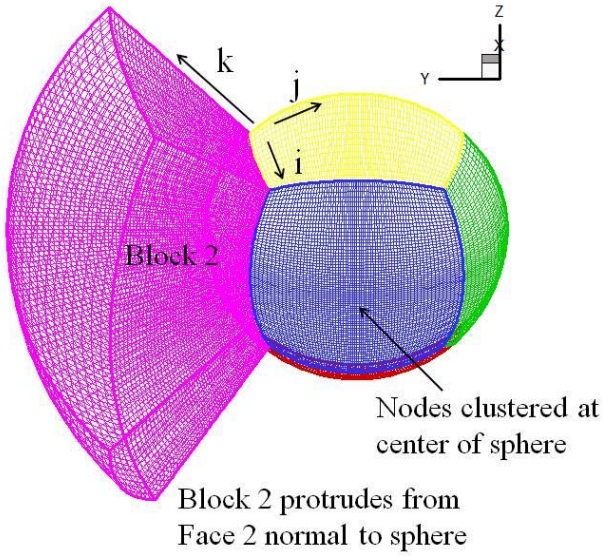

Figure 3.3. Three-Dimensional Domain Formed From Surface Grid by Protruding Out Normal to the Sphere Surface.

3.2. VALIDATION

A study is conducted in order to ensure that the results of this numerical work are consistent with available experimental results. In the first comparison, flow is simulated over the hemisphere with no injection or free-stream energy deposition. The free-stream Mach number is 6 and the free-stream pressure and temperature are selected to match the experimental condition in Reference [18]. A stable solution is obtained and the resulting pressure trace along the surface coordinate of the body, *s*, is shown in Figure 3.4 for the CFD and experimental results [18]. The data are taken at the symmetry plane of the body. In Figure 3.4, the static pressure on the surface, *p*, is non-dimensionalized with respect to the stagnation pressure, p_s. Figure 3.4 reveals that the results of the experiment and numerical simulation are in good agreement.

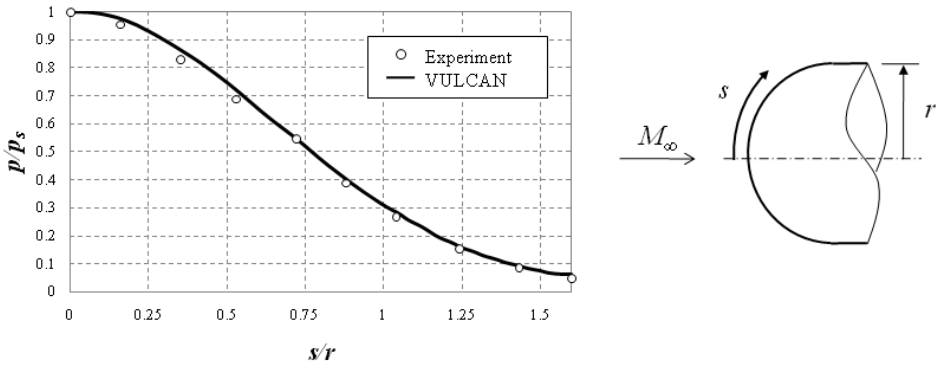

Figure 3.4. Pressure Trace on Surface with No Injection or Free-stream Energy Addition for Experiment and CFD Results.

A comparison between the CFD results and the experimental results in Reference [19], in which forward injection of air is present, is also made. In this case, the free-stream Mach number is 2.5 and the free-stream static temperature and pressure are again selected to match the conditions of the experiment. Air is injected forward from the stagnation point of the hemisphere at a Mach number of 1 and the ratio of the hemisphere diameter to the jet diameter, d/d_j, is 33.3. The ratios of the jet total pressure to the total pressure just aft of the bow shock for the base-line case with no injection, p_{tj}/p_{t2}, is 9.75

and the ratio of the jet total temperature to the free-stream total temperature, $T_{tj}/T_{t\infty}$, is 1.0. The results of the experiment and numerical simulation are shown in Figure 3.5. In Figure 3.5, the static pressure on the surface of the hemisphere at the symmetry plane is plotted verses the angle from the stagnation point and is non-dimensionalized with respect to p_{t2}. The numerical results do not converge to a steady solution; instead, the jet oscillates randomly in the lateral directions. The results shown in Figure 3.5 are therefore an ensemble average of the unsteady jet. The experimental and numerical results are sufficiently close to provide confidence in the ability of the CFD simulations to model such flows, particularly in terms of drag reduction and jet stabilization characteristics. Note that no information regarding experimental errors is given in Reference [19]. For both experiment and simulation, the pressure in the region adjacent to the jet decreases, compared to the base-line case with no injection, and hence the drag force decreases. The pressure then increases as the location from the jet increases until the pressure matches the base-line case.

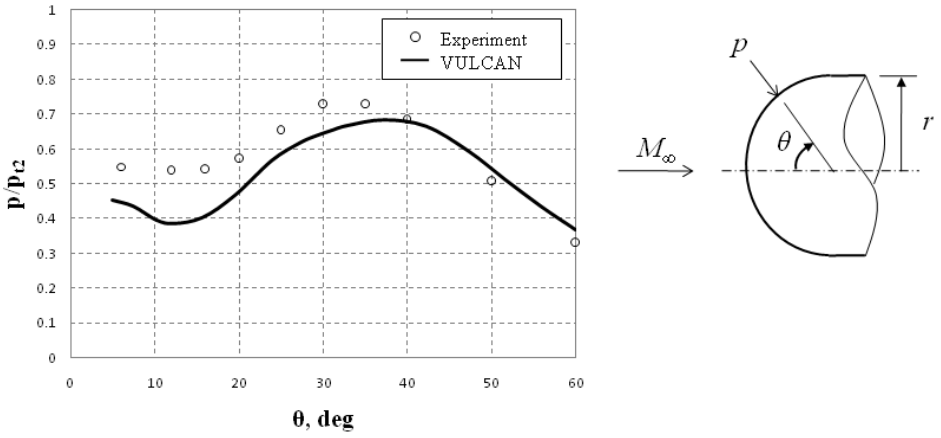

Figure 3.5. Pressure Trace on Surface with Forward Mass Injection of Air for Experiment and CFD Results.

4. RESULTS AND DISCUSSION

In this study, a series of numerical simulations were conducted in order to study innovative techniques for drag reduction and stability enhancement of upstream-directed injection. This section provides a summary of the techniques and conditions along with a discussion of the results in terms of flow-fields, drag reduction and stability. For comparison in terms of performance, a base-line case with no forward injection or energy deposition is first presented. Energy deposition with no forward injection is then investigated and the results of this full three-dimensional study are compared to a previous two-dimensional axi-symmetric study. Next, a study with forward injection alone is conducted and the unstable nature of injection is shown and discussed. Subsequently, a series of cases with swirled centered injection and swirled and non-swirled ring injection are conducted and the effects of these injection techniques on jet stability are presented. Lastly, the effects of coupling forward injection with free-stream energy deposition are examined.

4.1. BLUNT BODY WITH NO MASS INJECTION OR ENERGY DEPOSITION

Initially, a reference case with neither injection nor energy deposition is simulated. This reference case can be used as a base-line comparison when studying the effects of straight (non-swirled) gas injection, swirled gas injection, forward energy deposition, or a combination of techniques. Figure 4.1 shows a comparison between results obtained using an inviscid treatment of solid boundaries and results obtained for a full viscous and turbulent (Menter SST model) simulation. The two flow-fields are generated utilizing the same grid. The grid is generated in the same fashion as described before and the grid spacing is similar. However, the solutions shown in Figure 4.1 are obtained using a symmetry boundary condition on the y-plane (see Figure 3.2) which intersects the geometric center of the sphere. Each solution is taken to 40,000 iterations at which point the solution residual reduction reaches two orders of magnitude. The two cases compare well to each other, as well as to available experimental data. The data from the pressure contours are integrated over the surface of the sphere. The *x*-component of the integrated pressure is then taken as the pressure drag. Note that the

method for integration assumes that the surface elements have small skew. The drag forces obtained from the two flow-fields (inviscid and turbulent) are shown in Figure 4.1. There is a two percent difference between the drag forces, with the drag from the viscous turbulent solution being slightly larger than that of the inviscid flow-field. The Mach contours are also used to measure the shock standoff distance, Δ. For both solutions, the standoff distance is 0.0016 m. Note that the relatively course grid resolution in the axial direction prevents a precise measurement of this quantity. Based on experiments by Billig [20], the shock standoff distance for a sphere of diameter 0.02 m at Mach 6 should be 0.00147 m; the numerical results for standoff distance agree closely with this number. Similar comparisons are also made for the full three dimensional mesh as described in the discretization section of this report. In all cases, the results for the numerical simulation agree closely with published experimental results.

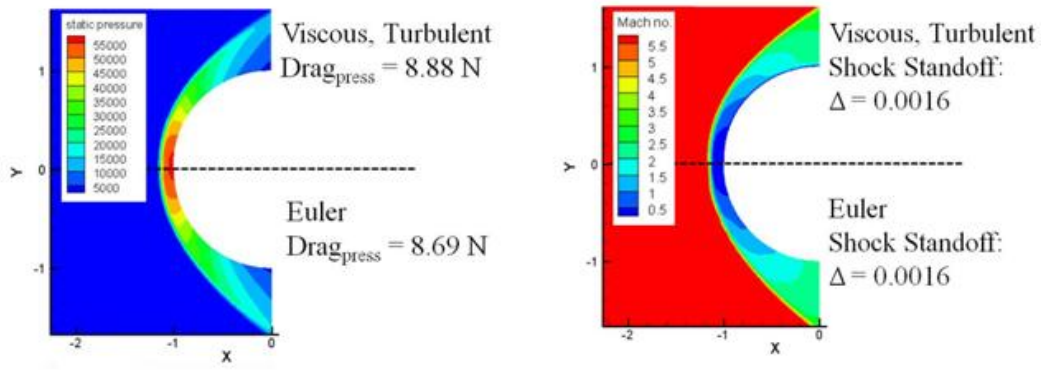

Figure 4.1. Pressure and Mach Contours Comparing Viscous, Turbulent Solution to Euler Solution.

4.2. EFFECT OF ENERGY DEPOSITION ON WAVE DRAG REDUCTION

As noted before, mass injection without energy deposition is unstable and hence the drag reduction results for a (2-D) axi-symmetric solution with mass injection (and no energy) will be inconsistent with the results of a full three-dimensional solution. Conversely energy deposition (and no injection) is stable and hence past studies of (2-D) axi-symmetric flow with energy deposition should predict the full three-dimensional

solutions studied in this work. Mach 10 flow over the hemispherical body at free-stream pressure and temperature of 1185.5 Pa and 231.24 K, respectively, (standard atmospheric conditions at 30 km altitude) is studied. A series of tests are conducted where energy is added to the free-stream at a fixed rate of 800 W and the location of the energy deposition forward of the nose of the body, *l*, is varied. The energy deposition location is non-dimensionalized with respect to the body diameter d and the resulting value, *l/d*, is varied from 0.5 to 2.5. Figure 4.2 shows the resulting Mach contour plots on the symmetry plane of the hemisphere for *l/d* of 1.0 and 2.0. As expected, the Mach number goes to zero at the region of energy deposition and the disturbance results in a conical shock. The Mach number in the region aft of the conical shock is reduced and the shock standoff distance increases. The pressure is integrated over the surface of the body and the resulting wave drag is obtained. The drag reduction is characterized by the drag ratio *R*:

$$R = \frac{D_{\text{mod}}}{D_{ref}} \tag{1}$$

where D_{mod} is the resulting drag after modifications including energy deposition and forward injection and D_{ref} is drag of the reference case with no injection or energy deposition. A drag ratio of $R = 1$ indicates zero drag reduction, where as a drag ratio of $R = 0.1$ indicates a 90% drag reduction from the base-line case. Another characterization of the effectiveness of energy deposition is the power effectiveness ratio *S*:

$$S = \frac{(D_{ref} - D_{\text{mod}} - T_j)V_\infty}{\dot{Q}} \tag{2}$$

where T_j is the thrust from the jet (which adds to the drag force), V_∞ is the free-stream velocity and $\dot{Q}$ is the rate of energy addition. The power effectiveness is a ratio of the propulsive power saved to the power required to modify the flow and a large value is desired. The jet thrust T_j is calculated as:

$$T_j = p_j A_j + \dot{m}_j u_j \tag{3}$$

where p_j is the static pressure of the jet, A_j is the area of the jet, $\dot{m}_j$ is the mass flow rate of the jet and u_j is the x-component of the jet velocity, all at the surface of the body where the jet is expelled from the body. T_j accounts for the reverse thrust due to the forward facing jet. For cases with energy deposition only, T_j is zero. The values of R and S are shown in Figure 4.2. For l/d = 2.0, R = 0.33 which indicates a 67% reduction in drag and S = 40.1 which indicates that for each unit of power deposited in the free-stream, approximately 40 units of power that would otherwise be used by the propulsion system to overcome the drag are saved.

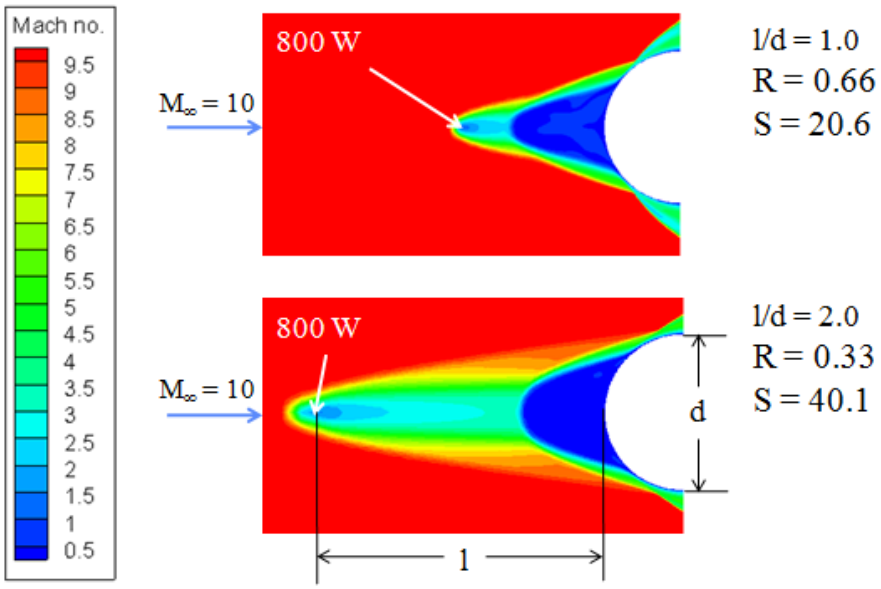

Figure 4.2. Mach Contour of Flow-Field Resulting from 800 W Energy Addition Rate at l/d = 1.0 and l/d = 2.0.

A similar axi-symmetric study was conducted by Riggins et al. [3]. Figure 4.3 compares this axi-symmetric solution to the full three-dimensional solution. The three-dimensional solution compares well to the axi-symmetric solution. The slight discrepancy can be accounted for by differences in the size and shape of the energy deposition. Both solutions indicate that as the location of the energy deposition forward

of the body increases, the resulting drag decreases until about l/d = 2.0. As l/d is increased further, the modified drag begins to increase from a minimum value.

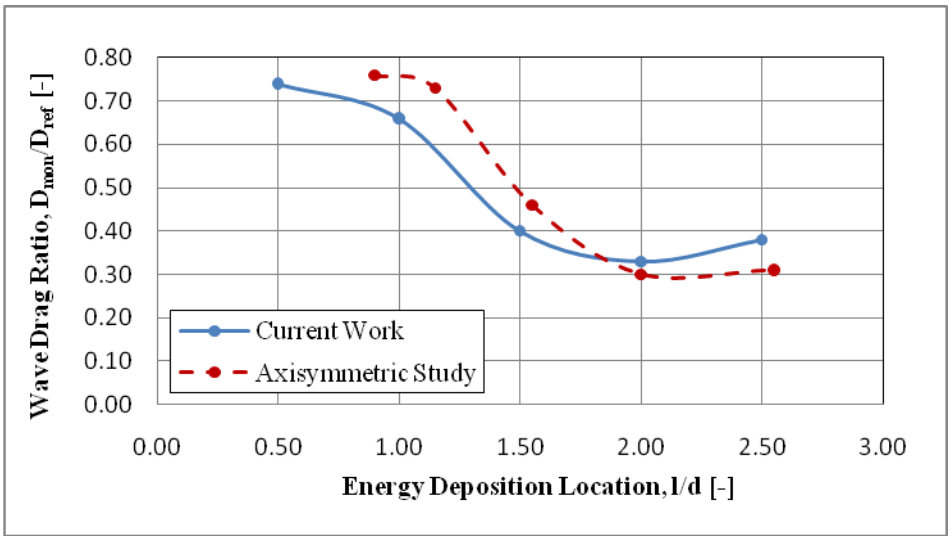

Figure 4.3. Comparison of Drag Reduction Ratio R vs. Energy Deposition Location, l/d.

4.3. EFFECT OF FORWARD INJECTION ON WAVE DRAG REDUCTION

One advantage of drag reduction on blunt bodies using forward injection alone, as opposed to energy deposition or a combination of energy deposition and injection is that the technology for forward mass injection is mature and can be implemented on systems today. Past numerical studies of forward injection have been two-dimensional and have either assumed a symmetry boundary condition [11] or have combined injection with energy deposition to increase the jet stability [19]. In this work, the stability of injection and the resulting drag reduction is investigated and the results are compared to a similar study employing a symmetry boundary condition. Using a similar mesh generating technique described above, VULCAN is used to obtain the solution of the flow over a half-hemisphere. The free-stream Mach number is 6.5 and the free-stream static pressure and temperature correspond to standard atmospheric conditions at a 30 km altitude. After flow is developed over the body, air is injected forward into the free-stream and the resulting flow-field is observed. The jet is characterized by several parameters including the Mach number M_j, the total pressure p_{tj} and temperature T_{tj}, and the ratio of the

diameter of the hemisphere to the diameter of the jet d/d_j. For this case, $M_j = 2$, $p_{tj} = 375$ kPa, $T_{tj} = 294$ K and $d/d_j = 46$. Note that mass is injected forward through a rectangular cross sectional area and the jet diameter is an equivalent diameter based on this cross sectional area.

Using the relations for isentropic nozzle flow, the mass flow rate of the injectant $\dot{m}_j$ as well as the static pressure of the injectant at the surface of the body p_j are calculated and the jet thrust is found to be $T_j = 0.047$ N. When calculating the modified drag on the body, the jet thrust is added to the axial component of the pressure integrated over the body surface. The reference drag (i.e. the drag force with no injection) is $D_{ref} = 10.34$ N. The drag penalty due to the forward injection is insignificant compared to the reference drag as well as to the modified drag.

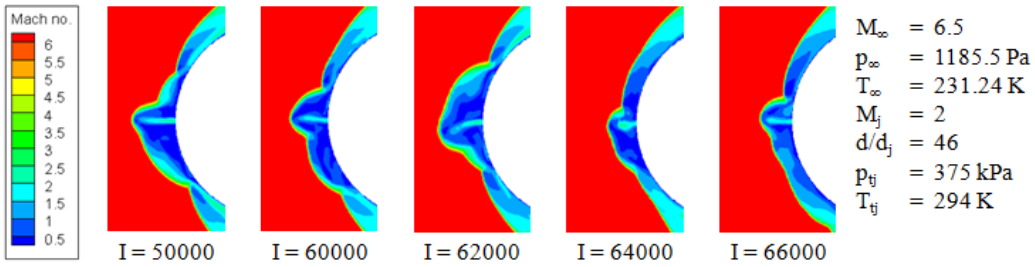

Figure 4.4. Mach Contours at Symmetry Plane Indicating Jet Instability.

Mach contours of the flow-field resulting from forward injection are shown in Figure 4.4. The contours are at the symmetry plane of the body and are shown for several iterations ranging from $I = 50{,}000$ to $I = 66{,}000$. The solution is not time accurate and exact details of the transient behavior are not predicted. However, by observing the solutions over several iterations, the instabilities associated with the jet can be seen. As predicted, the jet oscillates laterally and collapses back onto itself. What initially disturbs the jet and causes it to go unstable are the numerical oscillations which are inherent in any numerical discretization scheme. Once the jet becomes unstable however, the oscillations observed where those expected based on similar experimental tests, indicating that computational results are predicting actual physical oscillations. The drag

ratios ranged from 1.0 (zero drag reduction) to 0.9. Meyer et al. [11] conducted a numerical study with identical free-stream conditions as well as jet conditions. Meyer's study was two-dimensional and assumed a symmetry boundary condition. A steady solution was obtained in that study and the resulting drag ratio was 0.5. While Meyer's work was two-dimensional and the current work is three-dimensional, this alone does not account for the large discrepancies in drag reduction. The assumption of symmetry, for the case of a single jet injection out of the center of a body, is not valid and results in overly optimistic drag reduction.

4.4. EFFECTS OF ENERGY DEPOSITION ON STABILITY OF JET

Past studies have shown that the coupling of energy deposition with forward mass injection partially stabilized the jet. Khamooshi [21] studied this phenomenon for two-dimensional flows. Khamooshi's study did not assume a symmetry condition. The study observed the instability of a forward facing jet in a flow-field without energy deposition and then observed the improved stabilization of the jet after energy was added. This work studies similar effects for a three dimensional flow. The free-stream conditions as well as the parameters of the jet are identical to the flow-field studied in the previous section. Energy is deposited at a rate of 400 W into a small region two diameters forward of the nose. Mach contours of the resulting flow-field are shown in Figure 4.5 for several iterations. As noted before, while the exact transient behavior is not observed, the results at several different iterations give indications of the jet behavior. With the addition of energy deposition, the jet stability increases noticeably. The results are similar to the Khamooshi's two-dimensional study. A slight lateral instability remains but the instability in the axial direction where the jet collapse back onto itself in a cyclic pattern is eliminated.

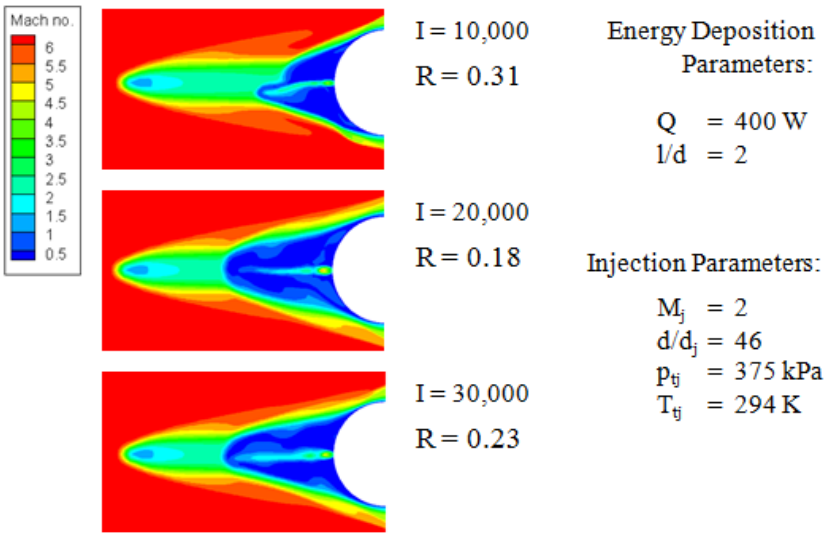

Figure 4.5. Mach Contours at Symmetry Plane Showing Effects of Energy Deposition on Jet Stability.

4.5. CENTERED INJECTION WITH SWIRL

As noted before, while energy deposition does provide a partial stabilization of the jet, it is desirable to stabilize the jet without energy addition. One method investigated for its potential to produce stable forward injection is to add a swirl component to the velocity. The motivation behind swirl injection is to gyroscopically stabilize the mass as it is injected forward, similar to a rifled bullet. The jet used to study forward, swirled injection has a Mach number of 2, a total pressure and temperature of 750 kPa and 294 K respectively and d/d_j = 63. Assuming isentropic flow in the injector system, the x-component of the velocity (i.e. the u-velocity or the axial velocity) of the jet at the body surface is 731 m/s in the negative x-direction. A velocity component normal to the surface (i.e. the lateral or swirl velocity) was added. Figure 4.6 shows a contour of the axial velocity of the jet as well as streamlines showing the lateral components of the jet. The swirl flow is injected at an angle of 12 degrees and the swirl-velocity component is 150 m/s at the surface of the body.

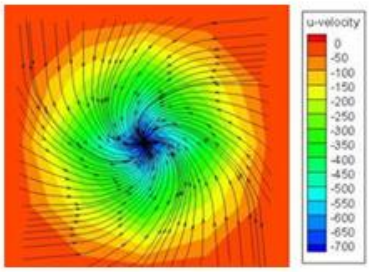

U-velocity = 731 m/s
Swirl-velocity = 150 m/s

Figure 4.6. Contour of Axial Velocity of Jet and Streamlines Showing Lateral Velocity Components of Jet.

Results of the swirl injection are compared to non-swirled injection as shown in Figure 4.7. Swirl appears to have minimal effect on jet stability. The drag reduction ratio is calculated every ten thousand iterations up to forty thousand iterations total. The drag reduction for non-swirled injection ranges from 20% to 3% less than the reference drag while the drag reduction for the swirled injection range from 24% to 1% less. While the swirl might provide slight gyroscopic stability to the jet itself, the effects of the swirl on the surrounding flow-field must be considered. Swirl induces asymmetric flow around the jet and hence pressure variations on either side of the jet triggering the instability mechanism previously described. For the particular parameters of this study, swirl does not improve jet stability and might in fact have a detrimental effect. However, the results of swirl on jet stability need to be tested for a range of jet parameters and swirl intensities before final conclusions can be made on effects of swirl in general.

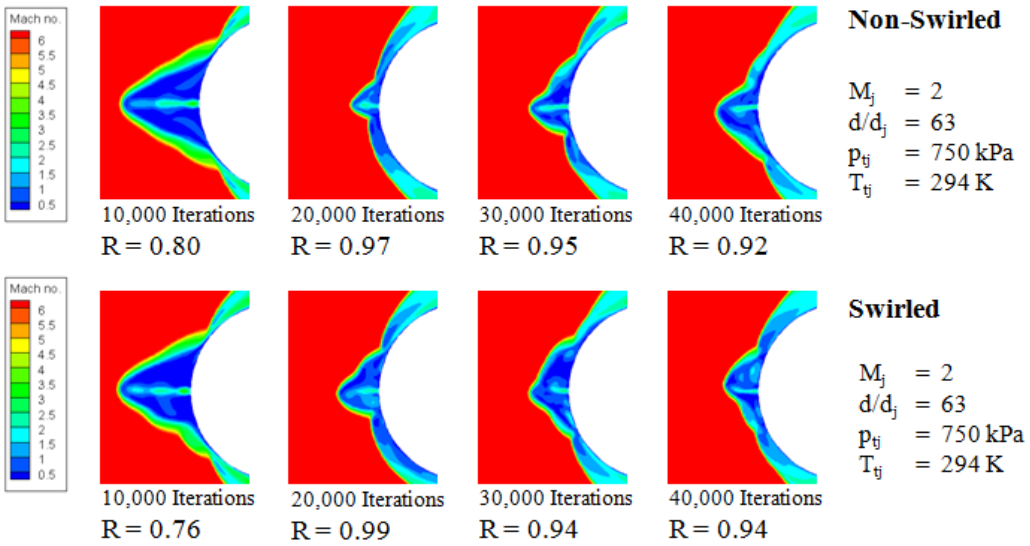

Figure 4.7. Comparison of Swirled and Non-Swirled Centered Injection.

4.6. EFFECTS OF RING INJECTION ON JET STABILITY

Another method investigated in the present work for increasing jet stability and improving drag reduction is annular-ring injection. The results of the ring injection technique are shown in Figure 4.8. The mass is injected forward in a ring pattern as shown in Figure 4.8a. A solution is obtained for the same free-stream conditions as the previous study of swirled and non-swirled centered injection: M_∞ = 6.5, P_∞ = 1185.5 Pa and T_∞ = 231.24 K. The jet parameters are also similar with M_j = 2, P_{tj} = 750 kPa and T_{tj} = 294 K. The ratio of the jet diameter to the diameter of the body d/d_j is 23. The jet diameter d_j is the effective diameter of the jet based on the cross sectional area of the ring. The cross sectional area is larger in the case of the ring injection compared to the centered injection and hence the mass flow rate of the injectant is greater, resulting in a larger drag penalty from the jet thrust.

The ring injection results in a stable jet with a constant drag of 10% less than the baseline drag. A Mach contour of the flow-field resulting from ring injection is shown in Figure 4.8b. The Mach contour shown is at the symmetry plane of the hemisphere. The ring injection creates an effective jet diameter which is larger than in the case of centered injection and the increased effective diameter might contribute to the jet stabilization.

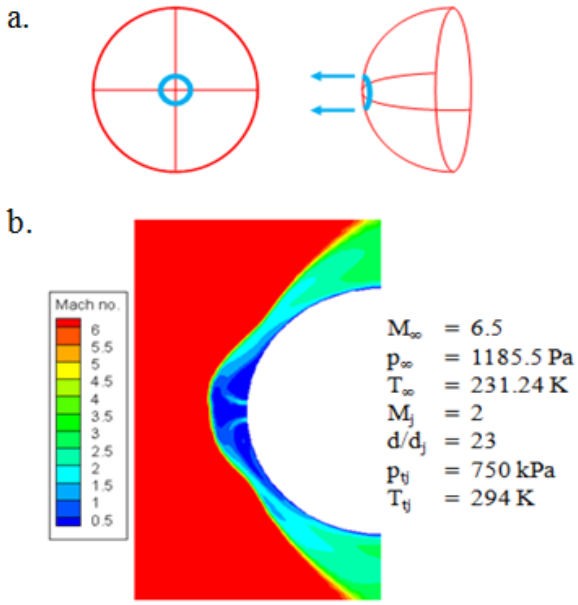

Figure 4.8. Ring Injection and the Resulting Flow-Field. a) Sketch of Ring Injection. b) Mach Contour of Modified Flow Resulting From Ring Injection.

Another explanation for the jet stabilization is that the flow on one side of the jet is isolated from the flow on the opposite side due to the void in the center of the ring in which no mass is injected. As discussed before, the jet destabilization results from a slight pressure variation on either side of the jet. A slight pressure decrease in one region of the flow creates an asymmetric distortion of the bow shock formed by the jet. This asymmetric distortion is such that the pressure decreases further in the said region and at the same time the pressure increases in the region opposite of the said region. With the ring injection, a reduction in pressure on one side of the jet with respect to the other does not result in an asymmetric bow shock which leads to an unstable jet. The ring injection case studied is at one particular set of jet parameters and free-stream conditions. The stabilization effects of the ring injection suggest that an axi-symmetric solution, which lends itself to parametric study, would reasonably predict the full three-dimensional solution.

To eliminate the increased injectant mass flow rate as the cause of the jet stabilization observed in the ring injection case, the centered, non-swirled injection case was repeated with and increase jet cross sectional area such that the injectant mass flow

rates of the two cases were identical. The centered, non-swirled injection, even with this increased injectant mass flow rate, still showed the unstable behavior where the jet oscillates and then collapses back onto itself.

4.7. EFFECTS OF SWIRLED RING INJECTION ON DRAG REDUCTION

Also studied are the effects of swirled ring injection on drag reduction. The motivation for swirled ring injection is the same as before; the rotation of the injectant could provide gyroscopic stabilization of the mass of the jet and prevent the jet from moving off centerline. Similarly to the study of centered swirl injection, a lateral velocity component is added to the jet by angling it 12 degrees. The results of the swirled ring injection technique are shown in Figure 4.9. Figure 4.9a shows a velocity contour of the axial component of swirled ring injection with streamlines showing the lateral velocity components. The axial velocity of the jet is 731 m/s and the lateral, or swirl, velocity is 150 m/s. The remaining parameters of the swirled ring injection are identical to the non-swirled ring injection, including the free-stream conditions: M_∞ = 6.5, P_∞ = 1185.5 Pa and T_∞ = 231.24 K and the jet parameters: M_j = 2, P_{tj} = 750 kPa, T_{tj} = 294 K and d/d_j = 23. A Mach contour of the resulting flow-field due to swirled ring injection at the symmetry plane of the hemisphere is shown in Figure 4.9b. The resulting flow is stable with a near constant drag reduction of 8%. Shown in Figure 4.10 is a comparison between the swirled and non-swirled ring injection. Based on the previous study of swirled and non-swirled centered injection and the conclusion that the swirl provides no stabilization, together with the fact that the flow conditions for both the centered and ring injection cases are similar, it is concluded that the reason for stabilization of the swirled ring injection is the ring injection pattern and not the swirl. The asymmetry of the swirled jet is evident in both Figure 4.9b. and Figure 4.10. This asymmetry results in pressure variations on the sides of the jet and could result in a slight destabilization of swirled ring jet compared to the non-swirled ring jet. The asymmetry of the swirled ring injection also causes a distortion of the bow shock formed at the end of the jet. By comparing the non-swirled and swirled injection results in Figure 4.10, it can be seen that the distorted bow shock of the swirled jet impinges the body to a greater extent compared

to the non-swirled injection. This fact can explain the higher drag observed in the swirled injection compared to non-swirled injection.

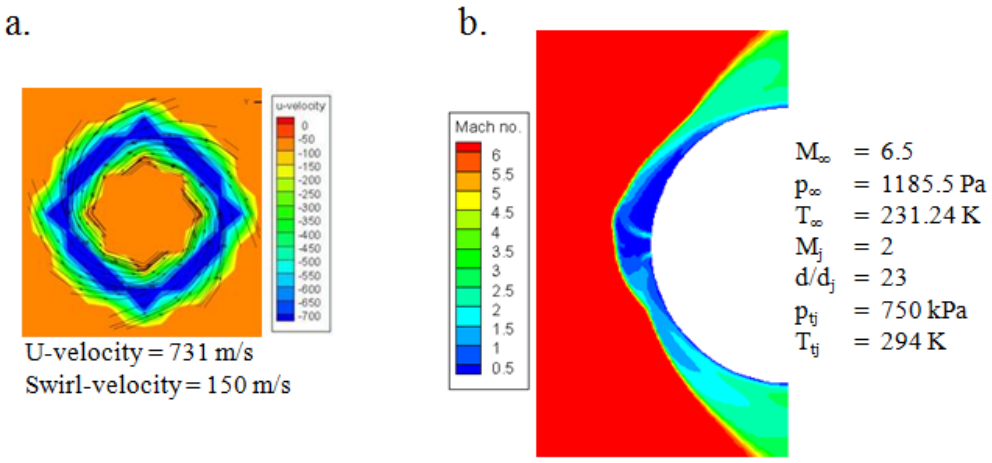

Figure 4.9. Swirled Ring Injection and the Resulting Flow-Field. a) Velocity Contour of Ring Injection with Streamlines Showing Swirl Component. b) Mach Contour of Modified Flow Resulting from Swirled Ring Injection.

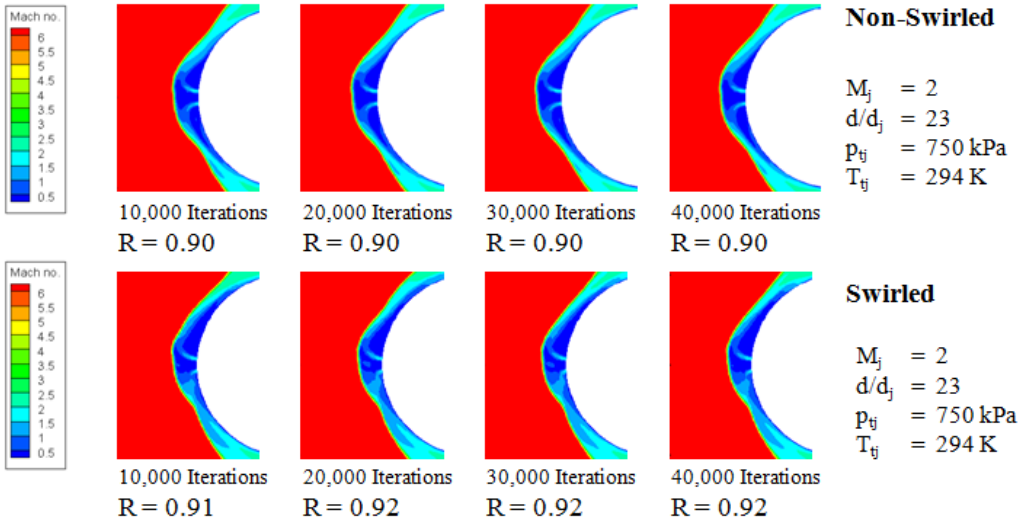

Figure 4.10. Comparison of Swirled and Non-Swirled Ring Injection.

4.8. COUPLED ENERGY DEPOSITION AND SWIRLED INJECTION

Earlier in this work, it was shown that free-stream energy deposition has a partial stabilizing effect on a centered non-swirled jet. The axial instability is minimized but the random lateral oscillation remains. Also investigated are the effects of energy deposition on the stability of a swirled centered injection. A simulation is conducted where a swirled centered jet is injected forward from the body while at the same time, energy is deposited in a small region forward of the nose at an *l/d* of 2 at a rate of 800 W. The parameters of the swirled jet are identical to the previous case of swirled centered injection: M_j = 2, P_{tj} = 750 kPa, T_{tj} = 294 K and d/d_j = 63. The free-stream conditions are also identical with a free-stream Mach number of 2 at standard atmospheric conditions corresponding to 30 km altitude. Shown in Figure 4.11 are Mach contours of the resulting flow-field due to swirled centered injection and energy deposition. The contours are at the symmetry plane of the hemisphere and are shown at several iterations. As in the case of non-swirled centered injection, the energy deposition provides a partial stabilization of the jet. Comparing the results for swirled and non-swirled centered injection coupled with energy deposition, it appears swirl has no significant effects. However, a range of swirl intensities must be tested before a conclusion can be made.

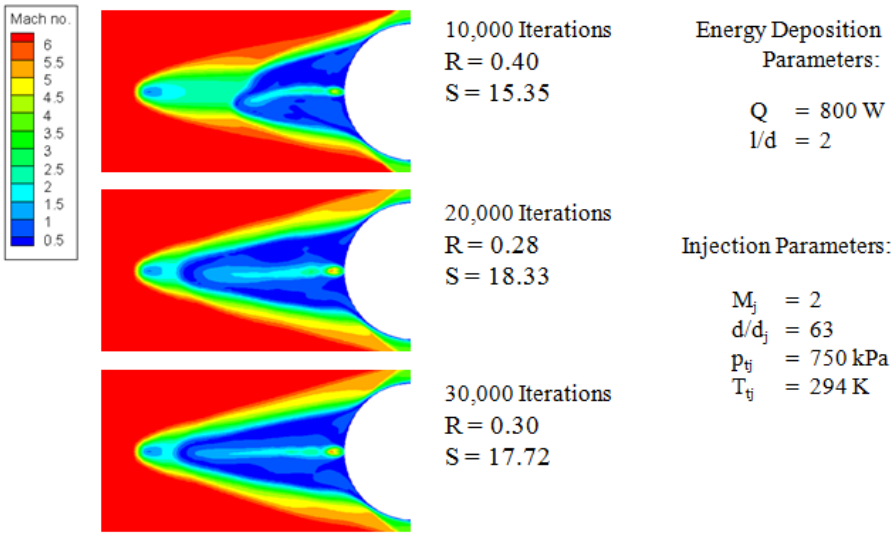

Figure 4.11. Mach Contours at Symmetry Plane Showing Effects of Energy Deposition on Stability of Swirled Centered Injection.

4.9. ENERGY DEPOSITION AND NON-SWIRLED RING INJECTION

The effects of free-stream energy deposition on non-swirled ring injection are presented in this section. A simulation is conducted at identical conditions to the case of non-swirled ring injection with no energy deposition, including the free-stream conditions: M_∞ = 6.5, P_∞ = 1185.5 Pa and T_∞ = 231.24 K and the jet parameters: M_j = 2, P_{tj} = 750 kPa, T_{tj} = 294 K and d/d_j = 23. The energy is deposited in a small region 2 diameters forward of the nose at a rate of 400 W. Shown in Figure 4.12 are Mach counters of the resulting flow-field due to energy deposition and non-swirled ring injection. The Mach contours are at the symmetry plane of the sphere and are shown over a range of iterations. As is evident in Figure 4.12, the jet exhibits unstable characteristics including random lateral oscillation. Also, the conical shock formed by the energy deposition does not impinge on the surface of the hemisphere as in the case of centered injection shown in Figure 4.11. The ring injection creates a larger effective jet diameter compared to centered injection which helps to deflect the conical shock away from the body. Shock impingement creates a region of high pressure on the surface and hence contributes to the drag. Ring injection potentially results in relatively lower drag compared to centered injection due to this deflection of the conical shock.

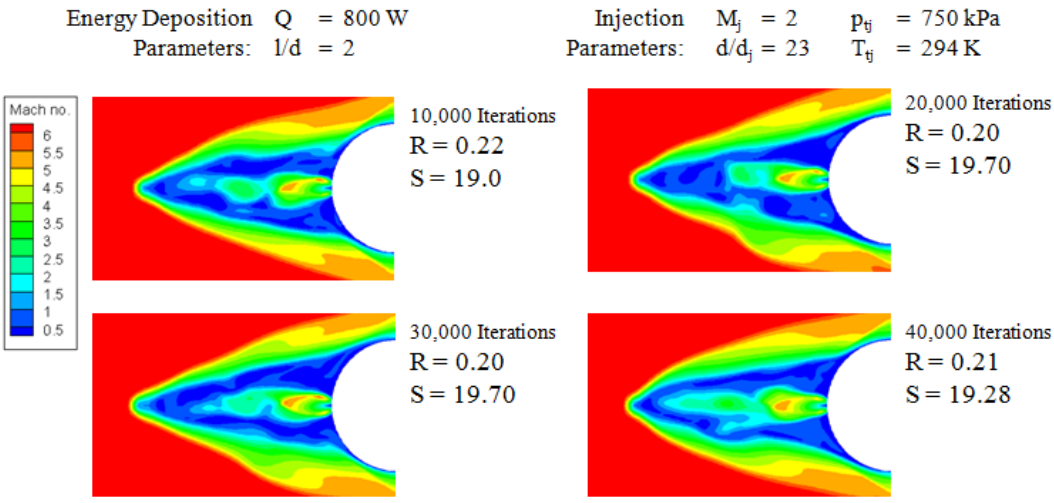

Figure 4.12. Mach Contours at Symmetry Plane Showing Effects of Coupled Energy Deposition and Non-Swirled Ring Injection.

5. CONCLUSIONS

Designing a hypersonic vehicle with a bunt nose, as opposed to the conventional vehicle configuration with high fineness ratio, mitigates the adverse effects associated with a sharp thin nose including excess heating, limited material selection and high bending stresses. Several methods of wave drag reduction on hypersonic blunt bodies were documented including the structural spike, forward mass injection and energy deposition. It was noted that a structural spike suffers from ablation which eliminates possible usage on long duration hypersonic cruise vehicles. It was also noted that, while energy deposition provides large drag reduction, the method increases heat transfer to the body. Also, energy deposition can only be implanted today in laboratories. These two considerations provided motivation for studying forward mass injection. Unfortunately, forward injection suffers from instability of the forward penetrating jet. This study then investigated methods for increasing the stability of forward mass injection.

A full three-dimensional computational fluid dynamic simulation of flow over a hemispherical body at hypersonic speeds was conducted. It was shown that previous numerical studies of forward injection, which assumed a symmetry boundary condition or an axi-symmetric condition, produce overly optimistic drag reduction results by eliminating the instability mechanism. It was also shown that the method of drag reduction by depositing energy in the free-stream is stable and that past axi-symmetric solutions predict the full three-dimensional solution. One method of increasing the stability of forward injection proposed in past work and studied using two-dimensional simulations was coupling forward injection with free-stream energy deposition. The same method was studied in this work for a full three-dimensional simulation and the results of both the two- and three-dimensional simulations were shown to be similar; the energy deposition partially stabilizes the jet by mitigating the axial instability while the lateral oscillation remains.

Methods for increasing jet stability without energy deposition were investigated including swirl injection and ring injection. The idea behind using swirl to increase jet stability was to provide gyroscopic stability to the jet and prevent it from moving off centerline. It was shown however that the swirl induces an asymmetric flow pattern

which triggers the jet instability mechanism. While swirl might cause gyroscopic stabilization of the jet, the asymmetric flow results in the effects of swirl on jet stability being negligible. On the other hand, it was shown that ring injection results in a stable jet with a constant drag reduction. The increased stability of the jet is due to one side of the jet being shielded from the other side. In the case of the centered jet, a small pressure variation on one side of the jet distorts the bow shock formed by the jet in such a way that the pressure on the other side of the jet increases. With the ring injection however, a small pressure disturbance on one side of the jet has minimal effect on the pressure on the opposite side. Also studied was the effect of combining swirled centered injection with energy deposition and it was found that the effects of swirl were again negligible. Lastly, upstream energy deposition was coupled with non-swirled ring injection. This study found that the ring injection, by creating a larger effective diameter, deflects the shock formed by the energy deposition and prevents the shock from impinging the body. The shock impingent creates a high pressure region on the surface and, by deflecting the shock, an even greater drag reduction can then be obtained.

BIBLIOGRAPHY

[1] Heppenheimer, T. A., Facing the Heat Barrier: A History of Hypersonics, NASA History Series, NASA SP-2007-4232.

[2] Shang, J. S., Hayes, J., Menart, J., "Hypersonic Flow over a Blunt Body with Plasma Injection," *Journal of Spacecraft and Rockets*, Vol. 39, No. 3, 2002, pp. 367-374.

[3] Riggins, D. W., Nelson, H. F., Johnson, E., "Blunt-Body Wave Drag Reduction Using Focused Energy Deposition," *AIAA Journal,* Vol. 37, No. 4, April 1999, pp. 460-467.

[4] Taylor, T. M., "On-Board Energy Management for High-Speed Vehicles: System and Component-Level Energy-Based Optimization and Analysis," Ph.D. Dissertation, Dept. of Mechanical and Aerospace Engineering, Univ. of Missouri – Rolla, Rolla, MO, 2007.

[5] Love, E. S., "The Effects of a Small Jet of Air Exhausting from the Nose of a Body of Revolution in Supersonic Flow," NACA RM L42119a, November 1942.

[6] Moeckel, W. E., "Flow Separation Ahead of Blunt Bodies at Supersonic Speeds," NACA TN 2418, July 1941.

[7] Stalder, J. R., Nielsen, H. V., "Heat Transfer from a Hemispherical-Cylinder Equipped with Flow-Separation Spikes," NACA TN 3287, September 1944.

[8] Gauer, M., Paull, A., "Numerical Investigation of a Spiked Blunt Nose Cone at Hypersonic Speeds," *Journal of Spacecraft and Rockets,* Vol. 45, No. 3, 2008, pp. 449-471.

[9] Stalder, J. R., Inouye, M., "A Method of Reducing Heat Transfer to Blunt Bodies by Air Injection," NACA RM A46827a, May 1946.

[10] Warren, H. M., "An Experimental Investigation of the Effect of Ejecting Coolant Gas at the Nose of a Blunt Body," GALCIT Hypersonic Research Report, Momorandum No. 47, December 1948.

[11] Meyer, B., Nelson, H. F., Riggins, D. W., "Hypersonic Drag and Heat-Transfer Reduction Using a Forward-Facing Jet," *Journal of Aircraft,* Vol. 38, No. 4, 2001, pp. 680-686.

[12] Romeo, D. J., and Sterrett, J. R., "Exploratory Investigation of the Effect of a Forward-Facing Jet on the Bow Shock of a Blunt Body into a Supersonic Free Stream," NASA TN D-1604, Feb. 1963.

[13] Tolle, F. F., "An Investigation of the Influence of a Forward Ejected Gas Stream on Hypersonic Flow About Blunt Bodies," Ph.D. Dissertation, Dept. of Aerospace and Mechanical Engineering, Univ. of Arizona, Tucson, AZ, 1973.

[14] Shneider, M. N., Macheret, S. H., Zaidi, S. H., Grigis, I. G., Miles, R. B., "Virtual Shapes in Supersonic Flow Control with Energy Addition," *Journal of Propulsion and Power*, Vol. 24, No. 4, 2008, pp. 900-914.

[15] Bracken, R. M., Hartley, C. S., Mann, G., Myrabo, L. N., Nagamatau, H. T., Shneider, M. N., and Raizer, Y. P., "Experimental and Computational Parametric Study of an "Air Spike" in Hypersonic Flow," AIAA Paper 2002-3784, July 2002.

[16] Bisek, N. J., Boyd, I. D., Poggie, J., "Numerical Study of Plasma-Assisted Aerodynamic Control for Hypersonic Vehicles," *Journal of Spacecraft and Rockets*, Vol. 46, No. 3, May-June 2009, pp. 568-576.

[17] Riggins, D., Taylor, T., Moorhouse, D., and Terhune, L., "Methods for the Design of Energy Efficient High-Speed Aerospace Vehicles," *Aeronautical Journal of the Royal Aeronautical Society,* Vol. 111, No. 1119, May 2007, pp. 297-309.

[18] Eaves, R. H., "An Empirical Correlation of Pressure on Blunt-Nosed Cylindrical Afterbodies at Hypersonic Mach Numbers," Von Karman Gas Dynamics Facility, Arnolds Engineering Development Center, Air Force Systems Command, Arnolds Air Force Station, Tennessee, 1968.

[19] Finley, P. J., "The Flow of a Jet From a Body Opposing a Supersonic Free Stream," *Journal of Fluid Mechanics*, Vol. 26, Part 2, pp. 337-368, 1965.

[20] Billig, F. S., "Shock Wave Shapes Around Spherical- and Cylindrical-Nosed Bodies," *Journal of Spacecraft and Rockets*, Vol. 4, No. 6, 1967, pp. 822-823.

[21] Khamooshi, A., Taylor, T, and Riggins, D., "Innovative Concepts for Large-Scale Drag and Heat Transfer Reduction in High-Speed Flows," *AIAA Journal*, Vol. 45, No. 10, pp. 2401-2413, October 2007.

VITA

Christopher David Marley was born in North Chicago Illinois. He graduated from Parkview High School in Springfield Missouri in 2004 and afterwards moved to Rolla Missouri to pursue an undergraduate degree at what was then the University of Missouri – Rolla. In 2009, he graduated from the Missouri University of Science and Technology with a Bachelors degree in Aerospace Engineering. After choosing to remain in Rolla for his graduate work, he finished his Masters degree in Aerospace Engineering in 2011.